Precision Spectroscopy with Frequency Combs at 3.4 μm

Esther Baumann*, Fabrizio R. Giorgetta, William C. Swann, Alex M. Zolot, Ian Coddington, and Nathan R. Newbury

NIST, 325 Broadway, Boulder, CO, USA 80305

ABSTRACT

We discuss precision spectroscopy with a comb-based spectrometer at 3.4 μm. Our goal is to explore comb-based spectroscopy as an alternative method for fast, highly resolved, accurate measurements of gas line shapes. The spectrometer uses dual 1.5 μm frequency combs down converted to 3.4 μm via difference frequency generation (DFG) with a stabilized 1 μm fiber laser. One 3.4 μm comb is transmitted through methane and heterodyned against the second, offset comb to measure the gas absorption and dispersion. Doppler-broadened methane spectral lines are measured to below 1 MHz uncertainty. We also discuss the higher sensitivity alternative of a comb-assisted swept-laser DFG spectrometer.

1. INTRODUCTION

Optical frequency combs (OFCs) have proven to be a powerful tool in a diverse range of applications, including molecular spectroscopy. They can be used directly as a broadband source or as frequency reference in swept laser measurements [1-15]. Here we explore OFC-based direct spectroscopy as an alternative to high-resolution Fourier transform infrared spectroscopy (FTIR) for rapid, high-resolution, high-accuracy measurements of a gas. More specifically we apply coherent dual-comb spectroscopy, where one sensing OFC is transmitted through a sample while a second OFC is acting as a local oscillator (LO). From the detected multi-heterodyne beat [6] the phase and amplitude response of the sample imprinted on the sensing OFC is extracted. In the time domain, this approach is analogous to asymmetric or dispersive Fourier transform spectroscopy but with the advantage of very high resolution, a collimated laser source, and no mechanical moving parts. For high accuracy the intrinsic frequency axis of the OFC needs to be extracted, which can only be achieved if the detection method fully resolves the OFC teeth. Fully resolved dual-comb spectroscopy was already demonstrated in the near infrared [8]. Today's most conventional OFC sources cover the visible to near-infrared portion (up to 2 μm) of the spectrum and do not extend out to longer mid-infrared (MIR) wavelengths; however, this spectral region is of special interest to molecular spectroscopy because the fundamental C-H stretch absorption lines lie in the 2 μm – 5 μm region. Therefore, there have been numerous efforts to extend OFCs to the MIR to support spectroscopic applications [3, 4, 13, 16-18]. Our approach to access the 3.4 um region is via difference frequency generation (DFG) between two 1.56 μm fiber laser OFCs and a 1064 nm cw fiber laser in a nonlinear periodically-poled lithium niobate (PPLN) crystal. Both the 1064 nm laser and OFCs are referenced back to a Hydrogen maser through a third self-referenced OFC. Therefore, the absolute frequency axis for the 3.4 μm OFCs is known. Line center measurements of Doppler broadened ro-vibrational absorption lines of the C-H stretch in the methane (CH_4) v_3 band around 3.4 μm have an uncertainty well below 1 MHz. This frequency accuracy is a significant improvement compared to FTIR systems. Compared to saturated absorption techniques, the dual-comb spectrometer allows for simultaneous measurement of multiple groups of lines, can be performed at higher pressures, and does not require a strong saturating laser beam but is about 10 times less accurate.

*esther.baumann@boulder.nist.gov; phone (303)497-3789, www.nist.gov

2. RESOLVED COHERENT DUAL-COMB SPECTROMETER

2.1 Setup

The setup for coherent dual-comb spectroscopy at 3.4 μm is shown schematically in Figure 1. It makes use of a signal OFC and a LO OFC at 1.56 μm with repetition frequencies $f_{r,S} \approx f_{r,LO} \approx 100$ MHz that differ slightly by $\Delta f_r = f_{r,S} - f_{r,LO} \approx 1.5$ kHz. The combs are tightly phase locked together with less than a radian of optical phase noise (integrated from 1 Hz to the Nyquist frequency $f_r/2$), as described in the next section. To access the 3.4 μm region we down convert the 1.56 μm dual-comb spectrometer via DFG in a 10 mm long PPLN crystal. To do so the pulses from each OFC are stretched from fs to ps width in 200 m of single-mode fiber, filtered with a 7 nm wide grating filter to match the PPLN phasematching bandwidth, amplified to 500 mW and combined in a fiber coupler with 500 mW of amplified 1064 nm light from a cw fiber laser. Both the cw 1064 nm fiber laser and fiber laser combs are referenced back to a Hydrogen maser through a third self-referenced frequency comb.

After the PPLNs the 1.56 μm and 1064 nm light is rejected by a Germanium (Ge) wedge, leaving a 20 μW (4 nW per tooth) 3.4 μm OFC in each branch, corresponding to a DFG conversion efficiency of $\sim 10^{-4}$/W. The 3.4 μm signal OFC passes through a 28 cm long cell filled with 200 mTorr of methane gas and is then combined with the unperturbed 3.4 μm LO OFC. Detection of the superimposed OFC electric fields with an InAs photodetector results in a multiheterodyne radio frequency (RF) comb (RFC), as seen in the left panel of Figure 2. The teeth spacing of the RFC equals the difference Δf_r in tooth spacing (repetition rate) of the signal and LO OFCs.
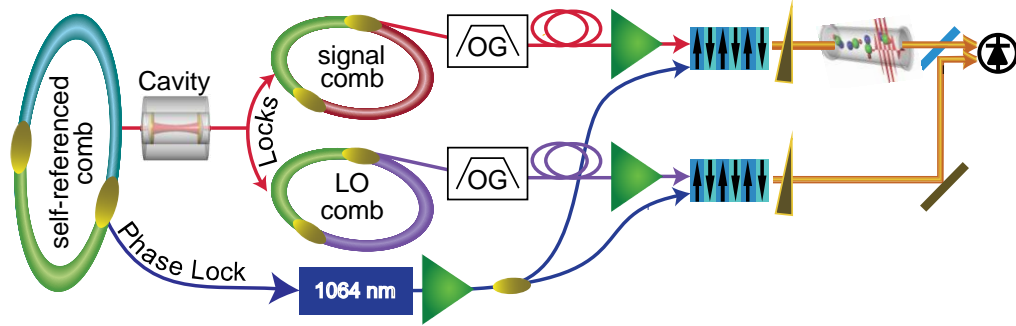

Figure 1: Schematic of dual-comb system. Two OFCs are tightly phase-locked together. The signal OFC probes a gas sample, and is then combined with the LO OFC on a detector. This results in a multiheterodyne RFC with tooth spacing equal to the difference in repetition rate of signal and LO comb. OG- Optical grating filter.

Provided that the OFC tooth linewidths are sufficiently narrow (as defined in the next paragraph), each RFC tooth is related to the heterodyne beat between one specific pair of OFC teeth (see Figure 2 (a)). If the RF spectrum is scaled appropriately by multiplying the frequency-axis by $f_r/\Delta f_r$ and applying an appropriate frequency offset, the scaled RF spectrum is proportional to $H(\nu)E_S(\nu)E_{LO}^*(\nu)$, where $E_S(\nu)$ and $E_{LO}(\nu)$ are the OFC electric field spectra, and $H(\nu)$ is the complex sample transmission at optical frequencies ν.

In a time-domain picture (Figure 2 (b)), the two OFCs are a pulse train. Because of the difference in repetition rates, there is a pulse-to-pulse shift of $\Delta t = f_{r,LO}^{-1} - f_{r,S}^{-1} \approx \Delta f_r/f_r^2$ in the arrival time of the signal-pulses with respect to the LO-pulses. The time offset between time-adjacent LO- and signal-pulses ranges from 0 to $f_{r,S}^{-1}$ as the LO pulses walk through the signal pulses, and then repeats. If the detector signal is digitized synchronously with $f_{r,LO}$, there are $N = f_{r,LO}/\Delta f_r$ digitized samples acquired in an update time $T_U = \Delta f_r^{-1}$ during which the LO pulse train completely walks through the signal pulse train. Such a data frame is related to the cross-correlation between the signal- and LO-pulses and we call it an interferogram in analogy to FTIR. The Fourier transform of the interferogram yields a spectrum that is equivalent to the RFC discussed earlier, proportional to $H(\nu)E_S(\nu)E_{LO}^*(\nu)$, has a resolution of f_r and covers an optical bandwidth of $(2\Delta T)^{-1}$ starting at an anchor frequency ν_0 where the teeth of both signal- and LO-OFC overlap.

The dual-comb spectrometer can be compared to FTIR: the light source is the signal OFC and the moving mirror is replaced with the LO OFC. With the sample placed in the signal arm, the interferogram is analogous to dispersive or

asymmetric FTIR [19, 20] rather than conventional FTIR where both the reference and the delayed beams pass through the sample. Due to this geometry, the gas sample's molecules are only excited by the signal OFC's pulses, and the interferogram is asymmetric relative to the centerburst (the interferogram peak at the time of overlapping signal- and LO-OFC pulses or, in FTIR, of zero path delay between reference and delay branches). In the frequency-domain, the consequence is that both phase and amplitude of the sample are measured (conventional FTIR only measures amplitude). We note that the combined speed and resolution of the dual-comb spectrometer would be challenging to achieve in an FTIR spectrometer, as it would require a 1.5 m long mirror displacement at a speed of ~2.5 km/s to measure a spectrum with 100 MHz resolution in 600 μs.
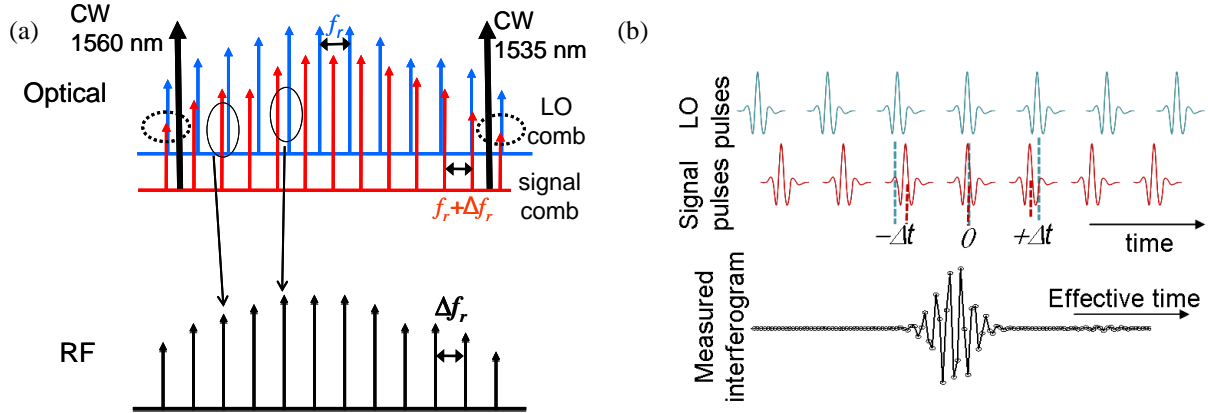

Figure 2: (a) Frequency-domain picture of coherent dual-comb spectroscopy illustrating the mapping of optical domain to RF domain. A signal OFC with a repetition rate / tooth spacing $f_{r,S}$ is mixed with a LO OFC (tooth spacing $f_{r,LO} = f_{r,S} + \Delta f_r$) on a photodetector, giving rise to a RFC with tooth spacing Δf_r. (b) Time-domain picture (not to scale) of coherent dual-comb spectroscopy illustrating its analogy to Fourier spectroscopy. A single interferogram is measured as the pulses of the LO- and signal-OFC walk through each other. The large 'wiggle' in the middle part of the interferogram is the centerburst and the small wiggles to the right are the result of free induction decay of a gas sample.

2.2 Adjustable Phase-locking of the combs

Our dual-comb spectrometer relies on a tight mutual phase-lock of the signal and LO OFCs. The residual linewidth between both OFCs has to be much narrower than the difference in repetition rates, Δf_r, to achieve well defined lines (or teeth) in the RFC, as is evident in Figure 2(a). In fact, even narrower OFC lines are required to allow for direct coherent signal averaging [9] since in this case the inverse linewidth sets an upper averaging time limit without needing to apply computationally intensive phase corrections. To achieve these narrow residual linewidths, each OFC is phase-locked to two cavity-stabilized cw fiber-lasers (at 1535 nm and 1560 nm), as was done in previous experiments [8, 9]. To lock the carrier frequency, an adjacent OFC tooth is stabilized to the 1560 nm laser with a phase-locked loop that feeds back to both a high-bandwidth extra-cavity acousto-optic modulator to achieve ~0.5 rad phase noise and a low bandwidth intra-cavity piezo-electric transducer (PZT), which compensates for slow drifts. To fully phase stabilize the OFCs, their repetition rates must be locked. We achieve this by phase-locking an adjacent comb tooth to the 1535 nm reference laser (see Figure 2 (a)) by feeding back to the current of the combs' pump diodes.
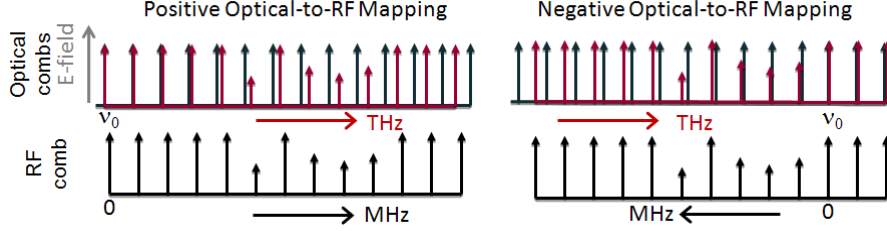
Figure 3: Sketch of positive and negative mapping of the optical to RF-domain

By requiring both combs to have overlapping teeth every few THz ($\Delta\nu_{span}$) and carefully choosing Δf_r by adjusting $f_{r,S}$ with an intracavity translation stage in the signal OFC, we force the signal and LO OFCs to obey $f_{r,S} = \Delta\nu_{span}/N$ and $f_{r,LO} = \Delta\nu_{span}/(N+1)$, where the integer $N = f_{r,LO}/\Delta f_r$ is the frame length discussed above. $\Delta\nu_{span}$ is chosen such that $\Delta\nu_{span}/2$, the measurement bandwidth is slightly broader than the width of the optical grating filter and PPLN phasematching to avoid aliasing effects. Having an integer number of samples, N, per frame allows for coherent co-adding of subsequent frames, thus increasing the signal-to-noise ratio (SNR), over a timescale limited by the inverse of the residual OFC linewidths. For even longer averaging times, the coherently co-added interferograms are phase-corrected before further summing.

In our earlier work [9], the teeth of both combs were phase-locked at the same RF frequency with regard to the reference lasers, and spectra always started at $\nu_0 = \nu_{1560} + f^{1560} + i\frac{\Delta\nu_{span}}{2}$ where i is an integer, ν_{1560}, ν_{1535} are the frequencies of the reference lasers, and f^{1535}, f^{1560} are the phase lock RF frequencies. In this case N (and correspondingly $\Delta\nu_{span}$) was fixed through $N = [(\nu_{1535} + f^{1535}) - (\nu_{1560} + f^{1560})]/f_{r,LO} - 1 \equiv N'$. In the current setup, we allow for differing phase-lock frequencies $f_{LO}^{15xx}, f_S^{15xx}$ in order to freely choose ν_0 and $\Delta\nu_{span}$ on a $f_{r,LO} \approx 100$ MHz grid. For given $f_{LO}^{1560}, f_{LO}^{1535}$, a desired $\nu_0 = \nu_{1560} + f_{LO}^{1560} + kf_{r,LO}$ and $\Delta\nu_{span} = (N+1)f_{r,LO}$ (where k, N are integers) are obtained by setting

$$f_S^{1560} = f_{LO}^{1560} - k\frac{f_{LO}}{N}$$
$$f_S^{1535} = f_{LO}^{1535} - k\frac{f_{LO}}{N} + \frac{(N-N')N'}{N^2}f_{LO}.$$

For the data presented below we set $N = 2^{16}$ for a 2^{16} sample interferogram repeating at a rate of $\Delta f_r = f_{LO}/N \approx$ 1.5 kHz, corresponding to a $\frac{\Delta\nu_{span}}{2} = (N+1)f_{LO}/2 \approx 3.3$ THz wide spectrum. k is set such that the optical spectrum shaped by the optical grating filter and PPLN phasematching peaks approximately 1.2 THz (corresponding to about 18 MHz in the RFC) above or below ν_0 (Figure 3).

3. MEASUREMENTS

3.1 Coherent dual-comb spectrometer with resolved comb teeth and spectral coverage around 3.4 μm

Figure 4 shows the measured heterodyne amplitude (shaped by the optical filter and PPLN phasematching window) centered at the Methane ν_3 band P(6) absorption lines. In Figure 4 (b) and (c), the individual RF beats between pairs of comb teeth are clearly visible. The optical frequency ν is linked to the RF frequency f by $\nu = \nu_{1064} - (\nu_0 \pm Nf)$ covering optical frequencies from $\nu_{1064} - \nu_0$ to $\nu_{1064} - (\nu_0 \pm \Delta\nu_{span}/2)$, where ν_{1064} is the frequency of the 1064 nm laser. As expected, the residual linewidth of the OFCs is conserved through the DFG. For 5.36 s of data acquisition (limited by the on-board memory of the digitizer), we find a time-bandwidth limited residual linewidth of 190 mHz, as seen in Figure 4 (c). The absolute tooth linewidth of the 3.4 μm is ~kHz limited by the absolute linewidth of the loosely stabilized 1064 nm laser and the light transport through ~10 meters of optical fiber.
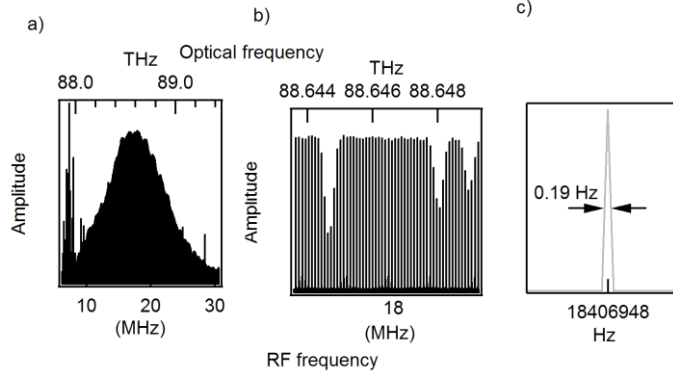
Figure 4: (a): Multiheterodyne comb measured at 3.4 µm centered on the methane P(6) lines, amplitude and phase; (b): Expanded view of $A_2^{(1)}$, $F_2^{(1)}$ and $E^{(1)}$ lines. (c) Further expanded view around 18.4 MHz showing an individual-comb tooth.

The total spectral coverage of our 3.4 µm dual-comb spectrometer is limited by the C-band Er-doped amplifiers to ~4.5 THz and covers P(11) to P(1), the Q-branch and R(1) to R(2) of the ν_3 band of methane.
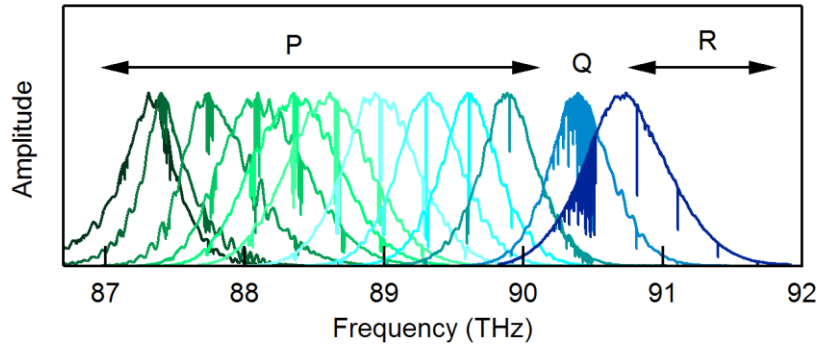

Figure 5: Covered spectral region of the dual-comb spectrometer. Each curve corresponds to one optical grating filter position and corresponding PPLN temperature settings.

In Figure 5 the optical filter and the temperature of the 10 mm long PPLN are tuned to cover the above mentioned ~4.5 THz. P(11) to P(2) (87-90 THz) are measured with a 29.9 µm poling period, the Q-branch and partial R-branch with a period of 30.2 µm. Each curve is measured for 13 minutes, and has an SNR of 3000 that is dark current limited by the InAs photodiode. Both the phase and amplitude of the signal are measured, although only the amplitude is shown in Figure 5. To extract the line center frequency from the 200 mTorr Doppler broadened methane absorption lines, we fit the measured absorbance (the ln of the amplitude signal) with a Gaussian function and the measured phase with the Dawson integral, correcting the baseline with a 3rd order polynomial for both amplitude and phase [22].

3.2 Systematics and Accuracy

There are a number of systematics errors that can influence the accuracy of the dual-comb spectrometer, most importantly mixing between comb teeth after passing through the methane cell that will distort the measured amplitude or phase lineshapes. We attribute observed nonlinearities to the photodetection since the optical pulse energy levels of the 3.4 µm combs are low enough that optical nonlinearites should be quite low. The impact of these nonlinearities on molecular line center determinations using the phase and amplitude measurement can be assessed by comparison to previous saturated-absorption measurements of the P(6) and P(7) lines with an accuracy of ~10 kHz [13]. These comparisons show offsets on the order of 1 MHz for phase and amplitude (Figure 6). (This offsets have their origin in the perturbed amplitude and phase of the individual comb teeth; a given tooth frequency remains unshifted).
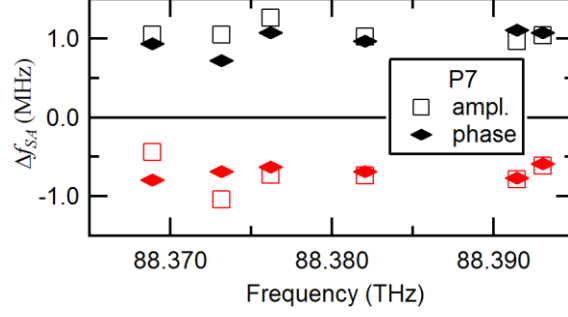
Figure 6: Systematic shifts for positive optical-to-rf mappings (red) and negative optical-to-rf mappings (black) in our measurements for the P(7) group. Δf_{SA} is the difference between our values and the saturated-absorption measurements of Takahata et al. [13].

The offsets are reversed by flipping the optical to RF mapping (Figure 3): for positive mapping, increasing RF frequencies correspond to increasing optical frequencies, whereas for negative mapping, increasing RF frequencies correspond to decreasing optical frequencies. As the RF spectra are 50 MHz wide (corresponding to 3.3 THz) and line centers are only extracted over a 500 kHz (corresponding to 30 GHz) span at the center of the 15 MHz (1 THz) wide optical spectrum, we can remove most of the nonlinearities by taking the mean value of a positive and a negative mapping measurement with the RFC signal spectrum centered at 18 MHz in both cases. Figure 6 shows amplitude and phase fit line center frequencies of the methane P(7) lines for positive and negative mapping. We then take the average of amplitude and phase line center frequencies for positive and negative mapping to obtain the absolute line center frequency. As seen in Figure **7**, our P(7) line center frequencies deviate by less than 300 kHz from the accepted saturated absorption truth data [13] for two sets taken 10 days apart (circles and triangles).
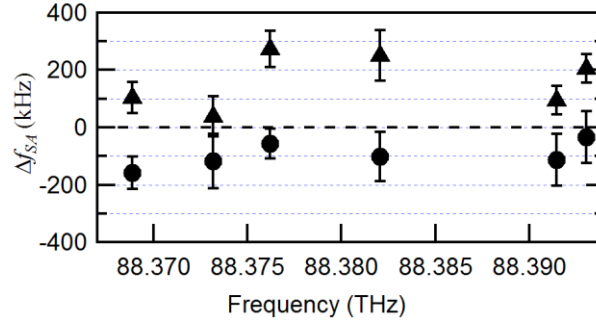

Figure 7: Fitted line center offsets relative to [13] for two data sets (triangle and circles) taken 10 days apart. The error bars represent the statistical uncertainty on the line center frequency from the curve fit.

3.3 Comparison to high resolution FTIR

As there are no saturated absorption measurements of the methane ν_3 band outside the P(6) and P(7) groups, we compare the line center frequencies from our data to FTIR data listed in the Hitran database [21]. The center frequencies of our measurement of the C-H stretch in the υ_3 band have a systematic uncertainty of 300 kHz [22] and lie within the 3 – 30 MHz uncertainty of the HITRAN database.

3.4 Combining swept cw laser spectroscopy and frequency combs

We also implemented comb assisted tunable cw laser spectroscopy for the 3.4 µm region. Tunable diode lasers offer a wide tuning range, rapid scan rates (e.g. > 1000 THz/s for Micro-electric Mechanical System (MEMS) external cavity diode lasers), and high output intensity. The latter makes those attractive compared to direct dual-comb spectroscopy, where typically low optical power levels limit the SNR. However the optical frequency of rapidly swept lasers is only poorly defined compared to the swept laser's linewidth. For precision measurements, it is thus necessary to either

precisely control [23-28] or accurately measure the instantaneous laser frequency. Here, frequency combs are used to track the phase of a swept MEMS laser [12, 29-32].
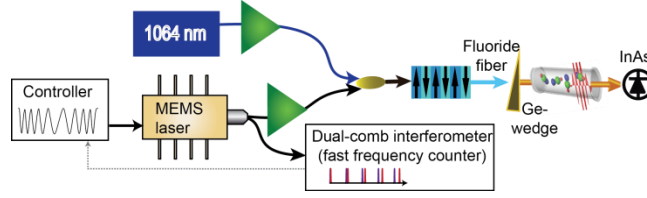

Figure 8: Setup for the comb assisted cw laser spectroscopy at 3.4 µm. Light from a MEMS 1.55 µm laser is down converted with a 1064 nm cw fiber laser to 3.4 µm. A small part of the MEMS diode's light is combined with the dual-comb spectrometer; the MEMS laser's phase and frequency is then extracted from the digitized heterodyne signal, allowing to accurately scale the frequency of the synchronously digitized 3.4 µm light. The PPLN is a high conversion efficiency ridge waveguided PPLN. A Ge-wedge filters out the remaining 1.55 µm and 1 µm light.

As seen in Figure 8 a fast tunable MEMS laser at 1.55 µm is combined with the stabilized 1064 nm light in fiber and coupled into a waveguided ridge PPLN (WPPLN) with a high conversion efficiency of 10%/W. The output beam is coupled into a fluoride fiber, to achieve a clean beam profile in the 3.4 µm light, and then collimated into a free space beam. The remaining 1.55 µm and 1 µm light is filtered out with a Ge-wedge. After passing through a methane gas cell, the 3.4 µm light is detected with an InAs diode. At the same time, a small part of the frequency modulated 1.55 µm MEMS light is split off and its frequency is measured with the dual-comb spectrometer. Using this data, the time axis of the 3.4 µm transmission measurement is converted into a frequency axis.
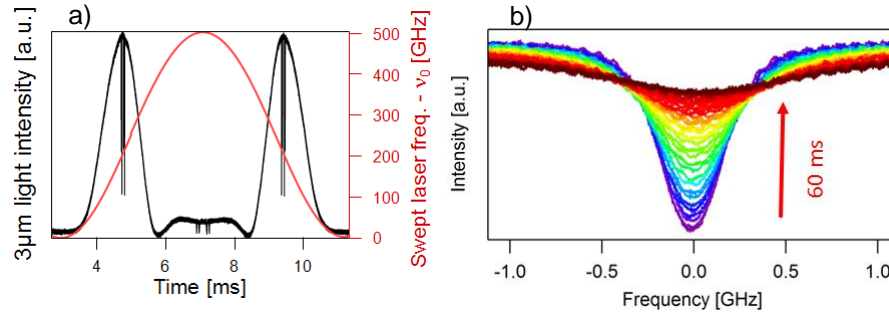

Figure 9: (a): Sinusoidal sample sweep with the WPPLN phase matching centered at P(6). (b): close-in on a single P(6) absorption line measured at a rate of 600 Hz over 60 ms while air was let into the methane cell. The increasing pressure broadening of the absorption line is clearly visible.

Figure 9 (a) shows a single period of the sinusoidaly frequency-modulated MEMS (red, right axis) and the corresponding 3.4 µm transmission (black, left axis) with the WPPLN phasematching temperature centered around P(6). Compared to the 10 mm long crystals described in section 3 the WPPLN's phasematching bandwidth is narrower (~200 GHz); also, the transmission has the expected $sinc^2$ shape with the upper two P(7) lines visible close to the MEMS frequency turnaround close to 7 ms. For this measurement the maximum chirp rate for 1.55 µm diode close to the P(6) lines was 200 THz/s and the time to cover all P(6) lines was 120 µsec (~ 25 GHz). The Spectral SNR is ~$10000/\sqrt{Hz}$ (scaled to 100 MHz point spacing). The precision of the relative P(6) line center frequencies is 250 kHz for a single measurement (at the time of writing, we did not yet calibrate the absolute frequency axis). Potential nonlinearities in the transmission detection can be corrected for by taking the mean of the upchirp (~4.5 ms in Figure 9 (a)) and the downchirp (~9.5 ms) measurements. This also corrects for any residual time delays between the MEMS frequency measurement and the transmission measurement. Figure 9 (b) shows the time evolution tracked over 60 ms from a Doppler- to a pressure broadened methane line while opening the valve to the methane cell and thus exposing it to air. For this measurement, the laser was modulated at 300 Hz, resulting in a P(6) measurement every 1.7 ms. The pressure broadening of the initially Doppler broadened methane line is clearly visible. The fast measurement rate and high SNR of the presented

swept cw laser combined with the high precision of the dual-comb spectrometer are promising for future lineshape studies and investigations of dynamic processes.

4. CONCLUSION

We demonstrated DFG combs at ~3.4 µm with sub-Hz residual linewidths, a prerequisite to high-precision and high accuracy coherent dual-comb spectroscopy at a wavelength where many fundamental molecular absorption lines are situated. The systematic uncertainties of the extracted line center are 300 kHz or one part per thousand of the Doppler broadened line width. This data is the first molecular precision measurement carried out with a dual-comb spectrometer. The SNR achieved is ~$110/\sqrt{\text{Hz}}$ over a spectral range of 4.5 THz with 45000 spectral elements covering the P-, Q- and partial R-branch of the ν_3-band of methane. Preliminary measurements carried out with a tunable 3.4 µm source tracked with the dual comb spectrometer give an improved SNR compared to direct dual comb spectroscopy of ~$10000/\sqrt{\text{Hz}}$ and show potential to track fast time evolutions.

REFERENCES

[1] Gohle, C., Stein, B., Schliesser, A., Udem, T. and Hansch, T. W. Frequency comb vernier spectroscopy for broadband, high-resolution, high-sensitivity absorption and dispersion spectra. Phys. Rev. Lett. 99(26), 263902 (2007).

[2] Giaccari, P., Deschenes, J. D., Saucier, P., Genest, J. and Tremblay, P. Active Fourier-transform spectroscopy combining the direct rf beating of two fiber-based mode-locked lasers with a novel referencing method. Opt. Express 16(6), 4347–4365 (2008).

[3] Johnson, T. A. and Diddams, S. A. Mid-infrared upconversion spectroscopy based on a yb:fiber frequency comb. submitted (2011).

[4] Thorpe, M. and Ye, J. Cavity-enhanced direct frequency comb spectroscopy. Appl. Phys. B 91(3), 397–414 (2008).

[5] Adler, F., Thorpe, M. J., Cossel, K. C. and Ye, J. Cavity-enhanced direct frequency comb spectroscopy: Technology and applications. Ann. Rev. Anal. Chem. 3, 175 (2010).

[6] Keilmann, F., Gohle, C. and Holzwarth, R. Time-domain mid-infrared frequency-comb spectrometer. Opt. Lett. 29(13), 1542–1544 (2004).

[7] Schliesser, A., Brehm, M., Keilmann, F. and van der Weide, D. Frequency-comb infrared spectrometer for rapid, remote chemical sensing. Opt. Express 13(22), 9029–9038 (2005).

[8] Coddington, I., Swann, W. C. and Newbury, N. R. Coherent multiheterodyne spectroscopy using stabilized optical frequency combs. Phys. Rev. Lett. 100(1), 013902 (2008).

[9] Coddington, I., Swann, W. C. and Newbury, N. R. Time-domain spectroscopy of molecular free-induction decay in the infrared. Opt. Lett. 35, 1395–1397 (2010).

[10] Bernhardt, B., Ozawa, A., Jacquet, P., Jacquey, M., Kobayashi, Y., Udem, T., Holzwarth, R., Guelachvili, G., Hänsch, T. W. and Picqué, N. Cavity-enhanced dual-comb spectroscopy. Nature Photon. 4, 55–57 (2009).

[11] Deschenes, J. D., Giaccari, P. and Genest, J. Optical referencing technique with cw lasers as intermediate oscillators for continuous full delay range frequency comb interferometry. Opt. Express 18(22), 23358–23370 (2010).

[12] Giorgetta, F. R., Coddington, I., Baumann, E., Swann, W. C. and Newbury, N. R. Fast high-resolution spectroscopy of dynamic continuous-wave laser sources. Nature Photon. 4, 853–857 (2010).

[13] Takahata, K., Kobayashi, T., Sasada, H., Nakajima, Y., Inaba, H. and Hong, F.-L. Absolute frequency measurement of sub-doppler molecular lines using a 3.4-µm difference-frequency-generation spectrometer and a fiber-based frequency comb. Phys. Rev. A 80(3), 032518 (2009).

[14] Mazzotti, D., Cancio, P., Giusfredi, G., De Natale, P. and Prevedelli, M. Frequency-comb-based absolute frequency measurements in the mid-infrared with a difference-frequency spectrometer. Opt. Lett. 30(9), 997–999 (2005).

[15] Cancio, P., Bartalini, S., Borri, S., Galli, I., Gagliardi, G., Giusfredi, G., Maddaloni, P., Malara, P., Mazzotti, D. and De Natale, P. Frequency-comb-referenced mid-ir sources for next-generation environmental sensors. Applied Physics B: Lasers and Optics 102, 255–269 (2011).

[16] Erny, C., Moutzouris, K., Biegert, J., Kühlke, D., Adler, F., Leitenstorfer, A. and Keller, U. Mid-infrared difference-frequency generation of ultrashort pulses tunable between 3.2 and 4.8 μm from a compact fiber source. Opt. Lett. 32(9), 1138–1140 (2007).

[17] Maddaloni, P., Cancio, P. and De Natale, P. Optical comb generators for laser frequency measurement. Meas. Sci. Technol. 20(5), 052001 (2009).

[18] Bernhardt, B., Sorokin, E., Jacquet, P., Thon, R., Becker, T., Sorokina, I. T., Picqué, N. and Hänsch, T. W. Mid-infrared dual-comb spectroscopy with 2.4 μm Cr2+:ZnSe femtosecond lasers. Appl. Phys. B 100(1), 3–8 (2010).

[19] Birch, J. R. Dispersive fourier-transform spectroscopy. Mikrochimica Acta 3(1-6), 105–122 (1987).

[20] Almoayed, N. and Afsar, M. High-resolution absorption coefficient and refractive index spectra of carbon monoxide gas at millimeter and submillimeter wave-lengths. IEEE T. Instrum. Meas. 55(4), 1033–1037 (2006).

[21] Rothman, L. S., Gordon, I. E., Barbe, A., Benner, D. C., Bernath, P. E., Birk, M., Boudon, V., Brown, L. R., Campargue, A., Champion, J. P., Chance, K., Coudert, L. H., Dana, V., Devi, V. M., Fally, S., Flaud, J. M., Gamache, R. R., Goldman, A., Jacquemart, D., Kleiner, I., Lacome, N., Lafferty, W. J., Mandin, J. Y., Massie, S. T., Mikhailenko, S. N., Miller, C. E., Moazzen-Ahmadi, N., Naumenko, O. V., Nikitin, A. V., Orphal, J., Perevalov, V. I., Perrin, A., Predoi-Cross, A., Rinsland, C. P., Rotger, M., Simeckova, M., Smith, M. A. H., Sung, K., Tashkun, S. A., Tennyson, J., Toth, R. A., Vandaele, A. C. and Vander Auwera, J. The HITRAN 2008 molecular spectroscopic database. J. Quant. Spectrosc. Radiat. Transfer 110(9-10), 533–572 (2009).

[22] Baumann, E., Giorgetta, F. R., Swann, W. C., Zolot, A. M., Coddington, I. and Newbury, N. R. Accurate spectroscopy of the methane v_3 band with a mid-infrared coherent dual-comb spectrometer. submitted (2011).

[23] Schibli, T. R., Minoshima, K., Hong, F.-L., Inaba, H., Bitou, Y., Onae, A. and Matsumoto, H. Phase-locked widely tunable optical single-frequency generator based on a femtosecond comb. Opt. Lett. 30(17), 2323–2325 (2005).

[24] Kim, Y.-J., Jin, J., Kim, Y., Hyun, S. and Kim, S.-W. A wide-range optical frequency generator based on the frequency comb of a femtosecond laser. Opt. Express 16(1), 258–264 (2008).

[25] Jost, J., Hall, J. and Ye, J. Continuously tunable, precise, single frequency optical signal generator. Opt. Express 10(12), 515–520 (2002).

[26] Satyan, N., Vasilyev, A., Rakuljic, G., Leyva, V. and Yariv, A. Precise control of broadband frequency chirps using optoelectronic feedback. Opt. Express 17(18), 15991–15999 (2009).

[27] Barber, Z. W., Babbitt, W. R., Kaylor, B., Reibel, R. R. and Roos, P. A. Accuracy of active chirp linearization for broadband frequency modulated continuous wave ladar. Appl. Opt. 49(2), 213–219 (2010).

[28] Inaba, H., Ikegami, T., Hong, F.-L., Bitou, Y., Onae, A., Schibli, T. R., Minoshima, K. and Matsumoto, H. Doppler-free spectroscopy using a continuous-wave optical frequency synthesizer. Appl. Opt. 45(20), 4910–4915 (2006).

[29] Liu, T.-A., Shu, R.-H. and Peng, J.-L. Semi-automatic, octave-spanning optical frequency counter. Opt. Express 16(14), 10728–10735 (2008).

[30] Barber, Z. W., Giorgetta, F. R., Roos, P. A., Coddington, I., Dahl, J. R., Reibel, R. R., Greenfield, N. and Newbury, N. R. Characterization of an actively linearized ultra-broadband chirp laser with a fiber-laser optical frequency comb. Opt. Lett. 36(7), 1152–1154 (2011).

[31] Del'Haye, P., Arcizet, O., Gorodetsky, M. L., Holzwarth, R. and Kippenberg, T. J. Frequency comb assisted diode laser spectroscopy for measurement of microcavity dispersion. Nature Photon. 3(9), 529–533 (2009).

[32] Coddington, I., Giorgetta, F. R., Baumann, E., Swann, W. C. and Newbury, N. R. Characterizing fast arbitrary cw waveforms with 1500 THz/s instantaneous chirps. IEEE Journal of Selected Topics in Quantum Electronics IEEE Early Access (2011). Available online